nature materials

SUPPLEMENTARY INFORMATION

DOI: 10.1038/NMAT4222

Solid friction between soft filaments

Supplementary Methods:

Actin purification and handling: Monomeric G-actin was isolated from frozen chicken skeletal muscle (Pel-Freeze) following the standard protocol[1,2]. To eliminate any oligomers, G-actin was subsequently purified on a size exclusion column (Sephacryl S-200HR, GE Healthcare) and stored in G buffer (2 mM HEPES, 0.2 mM ATP, 0.2 mM $CaCl_2$, pH 7.5) at -80°. Filamentous F-actin was polymerized by dissolving G-actin monomers in F-Buffer (10 mM HEPES, 150 mM KCl, 2 mM $MgCl_2$, 1 mM DTT, pH 7.5). F-actin was labeled with Alexa-488-phalloidin (Molecular Probes) at an equi-molar dye to monomer ratio[3]. All samples were prepared in buffer containing 30% sucrose w/w, 20 mM phosphate pH 7.5 and either 200 or 400 mM KCl as indicated in the text. Sucrose slows the desorption rate of Alexa-488-phalloidin thus prolonging sample lifetimes[4]. To suppress photobleaching an oxygen scavenging system was used at final concentration of 5 mM DTT, 3 mg/ml glucose, 20 μg/ml glucose oxidase, and 3.5 μg/ml catalase. Gelsolin was purified from rabbit plasma (Pel-Freeze) according to previously published protocol[5].

Gelsolin coated beads: The actin filaments where attached to a silica bead using gelsolin, a protein that strongly binds to the filament's barbed end[6]. Gelsolin was covalently attached to silica beads using a modification of previously published protocol[6]. Carboxylated beads (10 mg of 1 μm diameter, Bangs Beads) were suspended in 1 mL of deionized water. The beads were centrifuged twice (1500 g for 5 minutes) and re-suspended in deionized water. Subsequently, they were washed three more times and each time were resuspended in 1 mL of 2-(N-morpholino) ethanesulfonic acid (MES) buffer (50 mM, pH 6.0). After the final spin, the beads were resuspended in 1 mL of MES buffer containing 0.4 mg 1-Ethyl-3-(3-dimethylaminopropyl) carbodiimide (EDC) and 0.6 mg N-hydroxysuccinimide (NHS). They were gently mixed on a slow rotator for 15 min, spun down twice to remove excess reagent, and resuspended in 0.5 mL of phosphate buffer (20 mM, pH 7.4). The coated beads were sonicated with a tip sonicator to reduce bead aggregation. At this time gelsolin (10-40 μg in phosphate buffer (0.5mL, 20 mM, pH 7.4)) was added to the beads. The resulting mixture was slowly stirred for 5 to 8 hours at 4°. The gelsolin coated beads were spun down twice to remove any

DOI: 10.1038/NMAT4222

unbound gelsolin and were re-suspended in phosphate buffer (20 mM, pH 7.4, 10 mg/ml BSA). When stored at 4^{o}, gelsolin labeled beads remained active for up to 3 months.

Since calcium affects gelsolin activity, the experiments were performed in presence of 1 μM $CaCl_2$. A trapped gelsolin coated bead was brought into the vicinity of an actin filament. Gelsolin initially attaches to the filament sideways. In a subsequent slower step it severs the filament resulting in an end-capped filament-bead construct. The time lag between sideways attachment and severing can be up to a few minutes. For filaments under tension the severing time is usually faster. Since gelsolin only binds the barbed end, the polarity of the attached filament is immediately known.

Microtubule preparation: Alexa-647 labeled tubulin was mixed with unlabeled tubulin at a 1:9 ratio to a final concentration of 1 mg/mL in buffer containing 80 mM PIPES pH 6.8, 1 mM EGTA, 2 mM $MgCl_2$) Polymerization was initiated by the addition of GMPCPP to a final concentration of 0.5 mM, and subsequently incubating at 37 ^{o}C for 2 hours. This mixture was aliquoted and frozen at -80 C for future use. Aliquots were diluted at a ratio of 3:20 and incubated at 37 ^{o}C for 2 hours. To cleave the C-terminus tails of tubulin subtilisin (P8038 Sigma) was added to a concentration of 1.5 mg/mL and incubated at 30 ^{o}C for 1 hour. Subtilisin activity was stopped by the addition of Phenylmethanesulfonyl fluoride to a final concentration of 1mM. Subsequently, the solution was then spun through a 60% glycerol solution cushion for 20 minutes at 80k rpm, and then resuspended to 0.15 mg/mL.

Instrumentation: Filament sliding experiments were performed using a time-shared optical trap. A trapping laser beam (1064 nm, Coherent Compass) was brought into the optical path of an inverted microscope (Nikon Eclipse Te2000-u) and focused with a 100X objective onto the image plane (Nikon PlanFlour, NA 1.3). To simultaneously trap multiple beads, a single beam was shared between different positions using an acousto-optic deflector (IntraAction-276HD)[7]. Bead position was determined with back focal plane interferometry using an 830 nm laser as a detection beam (Point Source, IFlex-2000)[8]. Trap stiffness was calibrated by analyzing the power spectrum of the bead position[8]**.** We detected position in two orthogonal directions corresponding to the directions in which we manipulate the traps. In all sliding experiments we pulled in the same direction using only 1 axis of the AOD, ensuring that force is along this direction. The lack of alignment between the QPD and the axis of the AOD makes

underestimate of the frictional force possible. However, computing the net force using both X and Y directions changed the force by less than 1%. Custom Labview software acquired images of sliding fluorescently labeled F-actin filaments while simultaneously recording the bead positions through a DAQ board (National Instruments PCI-6251). Cooled CCD device was used for image acquistion (Andor iKon-M).

Controlling polarity of filament bundle: A gelsolin coated bead can only be attached to the barbed end of a filament. In order to investigate the influence of filament polarity on sliding friction, we developed a strategy for attaching beads to both ends of the same filament. To create such a construct we first assemble two regular F-actin-bead constructs in which filaments are attached at their barbed ends. Subsequently, we bundle them together via the depletion forces (Fig. S3). To ensure that there is no slippage in this connection we add up to 7 short filaments to the bundle. The stability of such a construct was tested by placing it under a tension of 10 pN. The actin linkage could sustain this load without any detectable slippage. Controlling both ends of one filament allowed us to determine dependence of sliding friction on relative filament polarity.

Decorating F-actin filament with a PEG brush: F-actin filaments were coated with a PEG brush (mPEG-SPA, MW 2000, Nektar) which covalently binds to primary amines located on the filament surface by the N-Hydroxysuccinimide group. F-actin was polymerized and fluorescently labeled as described previously. Subsequently, filaments were mixed with a solution of mPEG-SPA in F-Buffer (pH=7.5) at a 10:1 PEG:actin monomer ratio. The solution was allowed to incubate at 4^{o} C for 3 hours.

Simulations of filament sliding: Sliding F-actin filament is modeled by a series of beads connected with springs. The filament is moving along a background sinusoidal potential, which is commensurate with the filament periodicity (Fig. S3A). Outside the region of the initial filament overlap the background potential is flat. The behavior of such a model is examined with overdamped molecular dynamics simulations[9]. We use dimensionless units in which forces are rescaled by k_BT/d, potential energy by k_BT, and time by $d^3\eta/k_BT$. The stiffness of the springs connecting the beads varies between 100-600 (k_BT/d^2), and the bead size is $0.6d$. The height of the potential varies between 2-15 k_BT. Simulations illustrate the mechanism by which the filament translocation takes place. Pulling the rightmost bead over the final barrier is

DOI: 10.1038/NMAT4222

accompanied by the soliton formation which carries local lattice compression leftwards along the filament contour length (Supplementary Movie S2). Once the soliton reaches the leftmost bead the entire filaments translocated by a one-lattice spacing.

Theoretical model of kink structure and dynamics: We outline intermediate steps that lead to Eq. (1) of main text. We exploit a perturbative approach that illustrates how, once formed, the kink can move retaining its static profile (see Ref. 10). We consider the driven stochastic sine-Gordon equation in the overdamped limit, appropriate for the experimental regime:

$$-\phi'' + \frac{1}{\lambda^2}\sin(\phi) = -\alpha\dot{\phi} - F + \eta(x,t), \tag{1}$$

where $\phi(x,t)$ is the displacement field, α is the drag coefficient, F is a constant applied force and $\eta(x,t)$ is a random fluctuating force modeling thermal noise. None of the terms on the right hand side were explicitly considered in the main text. If the pulling and random forces are small perturbations we can assume that the soliton retains it static shape and the effect of the force results in a translation over time of the position of the center of the soliton, denoted by the collective coordinate $X(t)$. To leading order in perturbation theory, we obtain a solution of the form:

$$\phi(x,t) = 4\tan^2\left(e^{\frac{x-X(t)}{\lambda}}\right) \tag{2}$$

Note that if inertia effects were present a Lorentz contraction of the kink width would be possible in the limit in which the kink moves close to the sound speed. However, these effects are not relevant in the overdamped limit. The total energy stored in the field can be obtained by substituting Eq. (2) into the following expression:

$$E = \int dx\left(\frac{1}{2}(\phi')^2 + \frac{1}{\lambda^2}(1-\cos\phi)\right) \tag{3}$$

If we assume for simplicity that $X(t)$=0 and denote the limits of integration by L_2 and L_1, we obtain:

$$E = \frac{4}{\lambda^2}\int_{L_1}^{L_2} dx\,\mathrm{sech}^2(x) \;= \frac{4}{\lambda^2}\tanh(L_2 - L_1) \tag{4}$$

This relation predicts how the sliding force will scale with filament overlap length.

Next we exploit a perturbative approach that illustrates how, once formed, the kink can move while retaining its static profile. When the overlap length is much smaller than the kink width, sliding takes place by a motion of the kink that we now model according to the overdamped dynamics of Eq. 1. First, we multiply both side of Eq. 1 with $\dot{\phi}$ and integrate with respect to x to obtain:

$$\int dx(-\dot{\phi}\phi'' + \frac{1}{\lambda^2}\dot{\phi}\sin(\phi)) = \int dx(-\alpha(\dot{\phi})^2 - F\dot{\phi} + \eta(x,t)\dot{\phi}) \quad (5)$$

Next we take a time derivative of Eq. 3, integrate by parts the first term and use the left hand side of Eq. 5 to obtain

$$\frac{dE}{dt} = \int dx(-\alpha(\dot{\phi})^2 - F\dot{\phi} + \eta(x,t)\dot{\phi}) \quad (6)$$

If the kink width is much smaller than the domain of integration and the center of kink is far from the boundary, E is approximately constant over time, making the left hand side of Eq. 6 equal to zero. Next, we substitute the ansatz (Eq. 2) for the kink profile $\phi(x,t)$ into Eq. 6 and obtain a Langevin equation for $X(t)$ where the statistics of the noise term must be suitably modified [1]:

$$\alpha\dot{X} - \frac{\pi}{4m}F + \frac{\pi}{4m}\xi = 0. \quad (7)$$

We can further add the gradient of the Peierl-Nabarro potential barrier $V_{PN}(X)$ on the right hand side of the above equation:

$$V_{PN}(X) = \frac{1}{2}E_{PN}(1 - \cos(x)). \quad (8)$$

Note however that E_{PN} is exponentially suppressed in the experimentally relevant limit for which the king width is large compared to lattice spacing[10]. Hence, within the simplified model considered here the kink can be viewed as particle whose spatial profile is described by the static solution in Eq. (2) translating at a speed $\dot{X}$. If the noise ξ in Eq. 7 is ignored or averages to zero, we obtain a constant average speed $\dot{X} \approx \frac{\pi}{4m\alpha}F$ (see Supplementary movie S2).

DOI: 10.1038/NMAT4222

Supplementary Figures

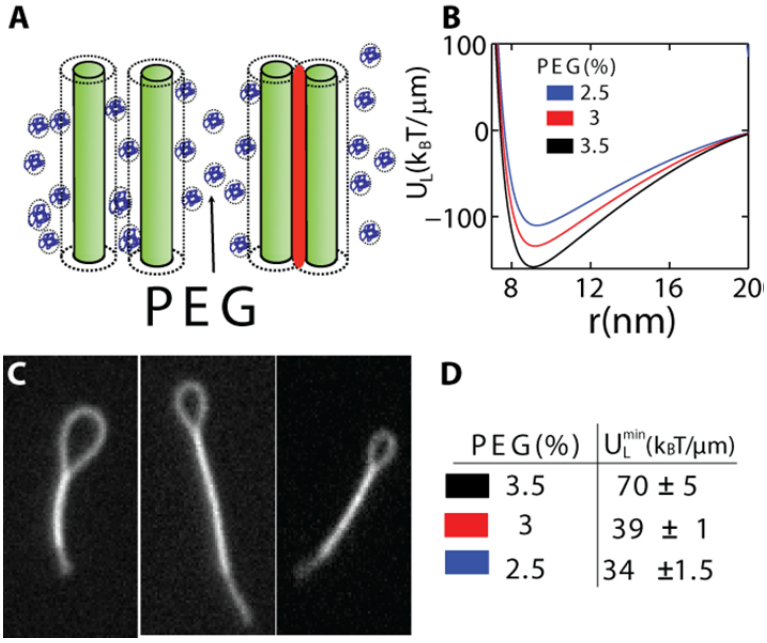

Figure 1. Adding non-adsorbing polymer to negatively charged actin filaments induces effective attractive interactions by the depletion mechanism. **A)** Adding non-adsorbing polymer exerts a uniform osmotic pressure on an isolated filament. A shell surrounding each filament excludes the center of mass of the depletion agent (PEG). As two filaments approach each other, the excluded volume shells overlap. Consequently there is an imbalance of osmotic pressure, which results in effective attractive interactions. The range and the strength of the depletion attraction can be controlled by changing the size and the concentration of the non-adsorbing polymers. **B)** Calculated pair potential between two aligned filaments at different PEG concentrations. **C)** In the presence of attractive interactions F-actin collapses into racquet-like structures. Images of actin racquets taken at three different PEG concentrations used for sliding experiments. Balancing adhesive interactions with filament elasticity estimates the binding energy per unit length. **D)** Adhesion energy as determined by analysis of racquet-like structures. The measured energies are significantly smaller then theoretical predictions in panel B due to the interpenetration of the filaments and depleting polymers as discussed in Ref. 11.

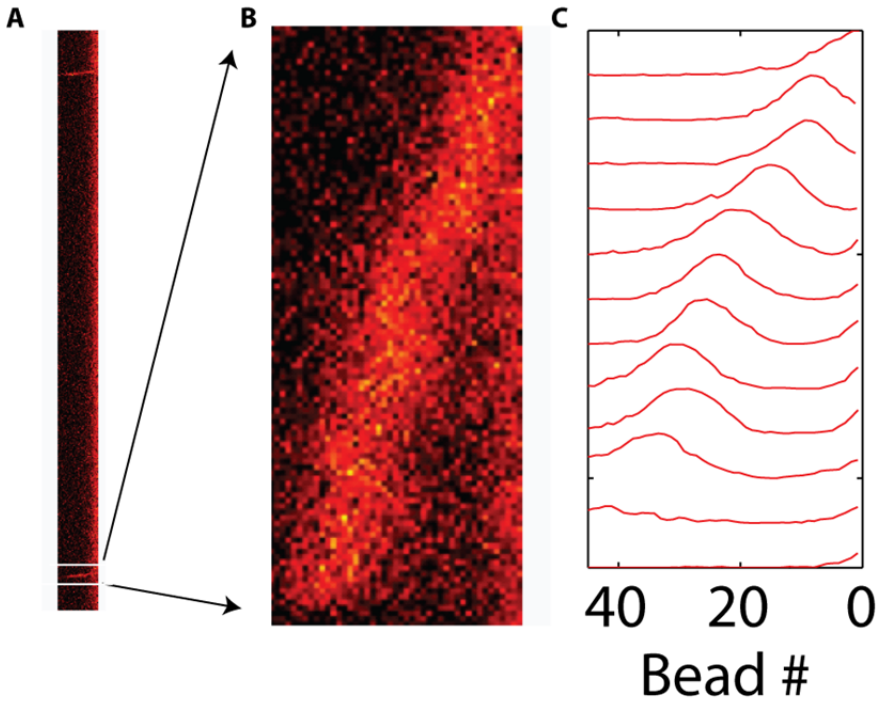

Supplementary Figure 2. Monomer hopping over a barrier is associated with the soliton formation which propagate along the filament. **A)** A kymograph illustrates temporal evolution of the tension (local filament compression) along the filament as it is pulled away from the periodic substrate. The pulling direction is to the right, while time evolution is downward. Each time a monomer is pulled over the rightmost barrier a soliton propagates along the filament enabling all the monomers to translate by one lattice unit. **B)** Zoomed in region demonstrates the propagation of a soliton, which carries local filament compression, along the filament contour. **C)** Another representation of filament configuration during propagation of a soliton. The *x*-axis represents the position along the filament contour while the *y*-axis is the local filament tension. For clarity filament conformations taken at different times are displaced along the *y*-axis. The dynamics of soliton propagation is illustrated in Movie S2.

DOI: 10.1038/NMAT4222

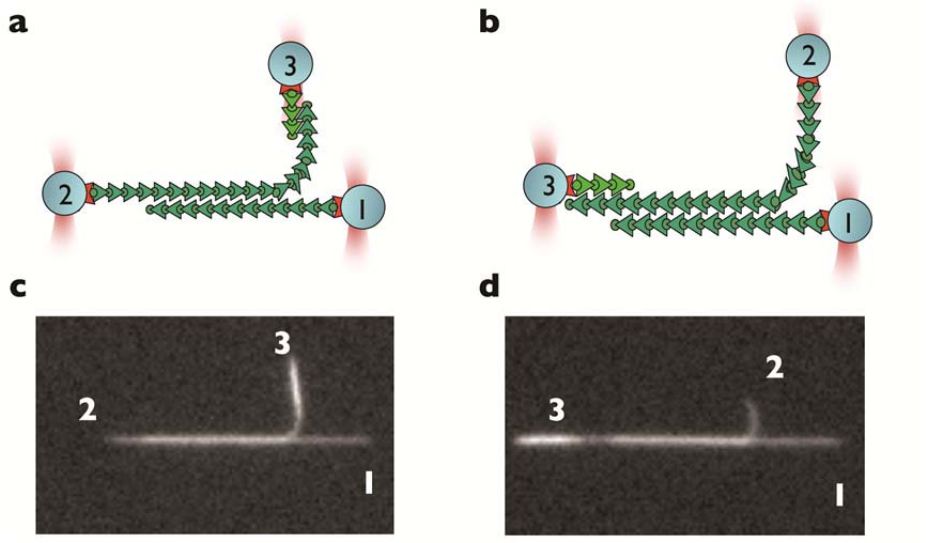

Supplementary Figure 3. Schematic of the three bead experimental setup used to measure the directional dependence of sliding friction. **(A)** Illustration of an actin bundle in which filaments have antiparallel configuration. The relative filament orientation is controlled by attaching beads to both ends of one filament as discussed in the supporting methods section. **(B)** Configuration used to measure sliding friction of filaments with same polarity. The bright region indicates the pointed end of a long actin filament which is bundled with a multifilament short bundle. The polarity of the filament bundle is switched by reversing the positions of bead 2 and 3. **(C)** Experimental configuration used to determine friction of filaments with same polarity. The brighter region in the vicinity of bead 3 indicates the short multifilament bundle which is attached to the pointed end of the long isolated actin filament attached to bead 2. **(D)** The experimental configuration corresponding to schematic in panel B is used to measure the sliding friction of parallel filaments.

Supplementary Tables

PEG(%)	A(pN)	v_o(nm/sec)	d(nm)
2.5	1.6 ± 0.3	6.4 ± 3	5.2 ± 1
3	1.4 ± 0.25	0.4 ± 0.3	5.8 ± 1
3.5	0.82 ± 0.6	2.E-05 ± 3.E-03	10 ± 7.4
2-AP	1.5 ± 0.4	0.27 ± 0.4	5.4 ± 1.4
2-P	1.5 ± 0.3	3.9 ± 2	5.4 ± 1

Supplementary Table 1. Experimentally measured force-velocity curves shown in Fig. 1D and Fig. 3B are fitted to the Tomlinson model. This provides an estimate for the spacing of the background periodic potential. Error bars are the 95% confidence intervals for each fit parameter

Velocity	λ_{exp}(nm)
40	1340
80	1300
180	1450

Supplementary Table 2. Comparison between the experimental kink width extracted from actin sliding runs done at three different pulling velocities

PEG(%)	λ_{exp}(nm)	λ_{theory}(nm)
3.5	820	2000 ± 400
3	1310	2800 ± 500
2.5	2170	3000 ± 600

Supplementary Table 3. Experimentally measured kink width extracted from actin pulling experiments is compared with theoretical estimates from our theoretical model. There are no adjustable parameters. Error bars for λ_{theory} are determined from standard error propagation of the parameters k, and U_o in the expression $\lambda^2 = kd^4/U_0$.

DOI: 10.1038/NMAT4222

Supplementary Movies

Supplementary Movie S1

Assembly of an actin filament bundle, and the subsequent pulling experiment designed to measure polymer friction. Two gelsolin coated beads, each with an actin filament attached, are held in place with optical traps. Bead 1 attached to filament 1 is located on the left, while bead 2 attached to the filament 2 is located on the right. Flow is used to establish a contact between the pointed end of filament 1 and bead 2. The gelsolin coated bead transiently binds sideways to the filament 1. Immediately upon binding, the flow in reversed in the opposite direction causing filament 2 to rotate by 180^{o} and bundle with filament 1 which is attached at both ends and thus is not affected by the external flow. Upon bundling, the region of increased brightness indicates the contact length between the two filaments. The gelsolin on bead 2 which is bound sideways to filament 1 eventually sever a portion of the filament off. At this point the filaments are free to slide. Bead 2 is moved at a constant velocity while simultaneously measuring force on the bead 1.The width of the image is 37 μm.

Supplementary Movie S2

Computer simulations reveal the dynamics of a filament translocation. The height of the bead in the background sinusoidal potential represents the local filament tension. Initially, the applied tension to the rightmost bead decays exponentially along the filament contour. At sufficiently large force or equivalently after long enough time, as the rightmost bead crosses the final barrier, a soliton like structure is formed. It travels along the entire filament contour allowing for the entire filament to translocate by unit spacing.

Supplementary Movie S3

Fluctuations of a bundled actin filament pair confined to quasi-2D. Both filaments have been coated with polyethylene glycol (MW 2,000). Unlike bare F-actin, PEG coated filaments exhibit significant sliding due to thermal fluctuations. The region of increased brightness indicates the location of the shorter filament which is bound to the longer one. Tracking the center of the short filament determines the mean square displacement. From there it is possible to determine the diffusion coefficient of the short filament. The width of the image is 12.7 μm and the duration of the movie is 180 seconds.

References:

1 Maclean-Fletcher, S. & Pollard, T. D. Identification of a factor in conventional muscle actin preparation which inhibts actin filament self-association. *Biochemical and Biophysical Research Communications* **96**, 18-27, doi:10.1016/0006-291x(80)91175-4 (1980).

2 Pardee, J. D. & Spudich, J. A. Purification of muscle actin. *Methods in Cell Biology* **24**, 271-289 (1982).

3 Brangwynne, C. P. *et al.* Bending dynamics of fluctuating biopolymers probed by automated high-resolution filament tracking. *Biophysical Journal* **93**, 346-359, doi:10.1529/biophysj.106.096966 (2007).

4 De La Cruz, E. M. & Pollard, T. D. Kinetics and thermodynamics of phalloidin binding to actin filaments from three divergent species. *Biochemistry* **35**, 14054-14061, doi:10.1021/bi961047t (1996).

5 Kurokawa, H., Fujii, W., Ohmi, K., Sakurai, T. & Nonomura, Y. Simple and rapid purification of brevin. *Biochemical and Biophysical Research Communications* **168**, 451-457, doi:10.1016/0006-291x(90)92342-w (1990).

6 Suzuki, N., Miyata, H., Ishiwata, S. & Kinosita, K. Preparation of bead-tailed actin filaments: Estimation of the torque produced by the sliding force in an in vitro motility assay. *Biophysical Journal* **70**, 401-408 (1996).

7 Molloy, J. E. Optical chopsticks: Digital synthesis of multiple optical traps. *Methods in Cell Biology, Vol 55* **55**, 205-216 (1998).

8 Allersma, M. W., Gittes, F., deCastro, M. J., Stewart, R. J. & Schmidt, C. F. Two-dimensional tracking of ncd motility by back focal plane interferometry. *Biophysical Journal* **74**, 1074-1085 (1998).

9 Frenkel, D. & Smit, B. *Understanding Molecular Simulation From Algorithms to Applications*. (Academic Press, 1996).

10 Braun, O. M. & Kivshar, Y. S. Nonlinear dynamics of the Frenkel-Kontorova model. *Physics Reports-Review Section of Physics Letters* **306**, 1-108, doi:10.1016/s0370-1573(98)00029-5 (1998).